JOURNAL OF NEUROPHYSIOLOGY
Vol. 66, No. 3, September 1991. *Printed in U.S.A.*

A Model of the T-Type Calcium Current and the Low-Threshold Spike in Thalamic Neurons

XIAO-JING WANG, JOHN RINZEL, AND MICHAEL A. ROGAWSKI
Mathematical Research Branch, National Institute of Diabetes and Digestive and Kidney Diseases, and Medical Neurology Branch, National Institute of Neurological Disorders and Stroke, National Institutes of Health, Bethesda, Maryland 20892

SUMMARY AND CONCLUSIONS

1. A model of the transient, low-threshold voltage-dependent (T-type) Ca^{2+} current is constructed using recent whole-cell voltage-clamp data from enzymatically isolated rat thalamocortical relay neurons. The T-type Ca^{2+} current is described according to the Hodgkin-Huxley scheme, using the m^3h format, with rate constants determined from the experimental data (22–24°C; extracellular Ca^{2+} concentration $[Ca^{2+}]_o$ = 3 mM).

2. The T-type Ca^{2+} current inactivates rapidly during maintained depolarization (time constant, $\tau_h \approx 20$ ms at −20 mV), yet recovery from inactivation is slow (time constant, $\tau_r \approx 270$ ms at −80 mV). To reconcile these observations, a two-step kinetic scheme is proposed for the inactivation gate. Each of the time constants in this scheme is voltage dependent, with a maximum at about −85 mV (45 ms for one and 275 ms for the other).

3. Numerical simulations of recovery in a two-pulse, voltage-clamp protocol compare favorably with experimental results obtained by Coulter et al. as well as those obtained in an independent series of experiments with guinea pig thalamic neurons ($[Ca^{2+}]_o$ = 10 mM).

4. For current-clamp simulations, a leakage current $g_L(V - V_L)$ is included; with V_L = −65 mV, the calculated resting membrane potential is −63 mV.

5. It is shown that the T-type Ca^{2+} current together with the leakage current suffices to describe the low-threshold spike (LTS), a slow, triangular-shaped depolarizing event that can be evoked only from relatively hyperpolarized membrane potentials and that underlies the burst firing of Na^+-dependent action potentials in thalamic neurons. Outward currents are not required to reproduce the basic shape of the LTS.

6. The LTS can be activated with either a depolarizing current step from a sufficiently hyperpolarized level or on termination of a hyperpolarizing current step. In either case, the amplitude of the LTS is a monotonically increasing, sigmoid-shaped function of the hyperpolarizing current step intensity.

7. Because of the slower kinetic step of the channel's inactivation gate, our model predicts that recovery of the LTS to greater than one-half amplitude would require a prolonged hyperpolarization of >100 ms (at body temperature). This imposes an upper limit (≈10 Hz) on the frequency of repetitive hyperpolarizations that can elicit a train of LTSs and hence on the frequency of any rhythm that requires LTS-mediated bursting of thalamic neurons. This finding is consistent with the views that the T-type Ca^{2+} current in thalamic neurons is critical to the generation of the 10-Hz spindle oscillations and that it may also play a role in the epileptic discharge during absence seizures.

INTRODUCTION

The thalamus has long been recognized as a key structure in the generation of brainwave rhythmicity (Steriade and Deschênes 1984; Steriade et al. 1990). Important progress in understanding the cellular basis of this pacemaker activity has come with an appreciation of the unique firing properties of thalamocortical relay neurons. These cells exhibit two distinct modes of firing depending on the membrane potential level (Deschênes et al. 1984; Jahnsen and Llinás 1984a,b). At normal resting potential, the cells transform suprathreshold input signals into trains of action potentials with high fidelity in what is referred to as "relay mode." However, on hyperpolarization there is an abrupt transition to phasic (burst) firing in which action potentials occur grouped into bursts. During drowsiness and slow-wave sleep, the burst firing of thalamic relay neurons plays an essential role in the generation of synchronized 8- to 10-Hz rhythmic oscillations ("spindling") in the cortical electroencephalogram. In addition, the stereotyped spike-and-wave discharges characteristic of absence (petit mal) seizures may also be dependent on synchronized thalamic bursting (Gloor 1984).

The following events are believed to occur in thalamic relay neurons during an episode of bursting oscillations. The relay neurons receive a barrage of long-duration (60–120 ms) inhibitory potentials at a frequency of 7–14 Hz, possibly from neurons in the nucleus reticularis. Some, but not all, of these transient hyperpolarizations result in deinactivation of broad, triangular-shaped depolarizing events, referred to as the low-threshold spikes (LTS). Each LTS, in turn, triggers a burst of fast action potentials that ride on its crest. As such, the LTS plays a critical role in linking synaptic input to intrinsic membrane mechanisms of bursting in the relay cell and in supporting the slow membrane oscillations underlying the spindling rhythm. In particular, it provides a cellular substrate for the postinhibitory rebound, which has been postulated as an important cellular property contributing to the rhythmicity in the thalamic neuronal network (Andersen and Andersson 1968).

It has recently been shown (Coulter et al. 1989; Crunelli et al. 1989; Hernández-Cruz and Pape 1989) that enzymatically isolated neuronal somata prepared from slices of the rat and guinea pig thalamus possess a prominent low-threshold, rapidly inactivating (T-type) Ca^{2+} current (Carbone and Lux 1984, 1987a; Fox et al. 1987a; Tsien et al. 1987) and, moreover, that the T-type Ca^{2+} current mediates the LTS recorded in these cells under current-clamp conditions (Suzuki and Rogawski 1989). These neurons have nearly ideal characteristics for voltage-clamp recording in that they are small; are roughly spherical in shape;

and have markedly truncated processes, allowing adequate spatial voltage control. Moreover, using the whole-cell patch-clamp technique, it is possible to perfuse the cells internally with impermeant cations to prevent contamination with outward currents. Consequently, accurate kinetic data have been acquired that allow a theoretical analysis of the T-type Ca^{2+} channel and its relationship to the LTS according to the paradigm of Hodgkin and Huxley (1952).

In the present work, we have constructed a minimal model of the LTS based on the recent voltage-clamp data, which show that the T-type Ca^{2+} current plus a leakage current are sufficient to reproduce accurately the LTS recorded under current-clamp conditions. In addition, we demonstrate that the slow recovery time of the T-type Ca^{2+} current I_T may be interpreted as a "bottleneck effect" related to a slow transition process of the inactivation gate of I_T. We discuss the relevance of this property in limiting the frequency of spindling oscillations and spike-and-wave discharges in animal models of absence seizures. Our work further indicates that K^+ currents are not required to reproduce the LTS itself; but such outward currents, as well as network properties, may contribute to determining the interval between burst events.

METHODS

Presentation of the model

Following Coulter et al. (1989), we model the T-type Ca^{2+} current in analogy with the fast sodium current of Hodgkin and Huxley (1952) according to

$$I_T = g_T m^3 h (V - V_{Ca}) \tag{1}$$

where g_T is the maximal conductance per unit area (expressed in mS/cm^2) and V_{Ca} is the reversal potential for calcium flux, here fixed at +120 mV. The value of g_T may be chosen to scale the amplitude of I_T to that measured in particular voltage-clamp experiments.

By hypothesis, m represents the fraction of channels for which one of the three activation gates is in its open state, "O," and h, the fraction of those with the inactivation gate in its open state. A channel is open if all of its four gates are in their O states. Each activation gate satisfies a two-state transition kinetics (Fig. 1A) with voltage-dependent rates α_m and β_m, so that

$$\dot{m} = \alpha_m(1 - m) - \beta_m m = (m_\infty - m)/\tau_m \tag{2}$$

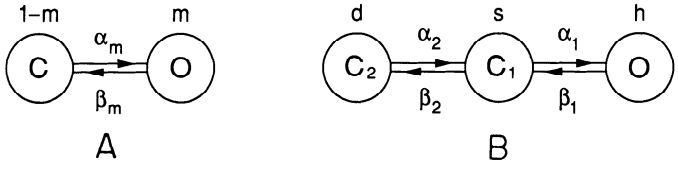

FIG. 1. Kinetic model of the T-type Ca^{2+} channel. *A*: an activation gate has 1st-order kinetics, with 1 open state O and 1 closed state *C*; the fraction of gates in O is m. *B*: the inactivation gate has kinetics with 2 steps and 3 states (1 open, O, and 2 closed, C_1 and C_2); the fraction of gates in each state is h, s, and d, respectively. Step between C_1 and O is assumed to be relatively fast. Step between 2 closed states C_1 and C_2 is much slower; it accounts for the slow recovery from inactivation. Model has 6 voltage-dependent kinetic rates: $\alpha_m(V)$, $\beta_m(V)$, $\alpha_1(V)$, $\beta_1(V)$, $\alpha_2(V)$, and $\beta_2(V)$. A T-type Ca^{2+} channel is open when its 3 independent activation gates and its inactivation gate are all in the open state. Total current satisfies *Eq. 1*.

where the dot notation is used to signify differentiation with respect to time. In *Eq. 2* we also allow for the alternative representation in terms of the functions $m_\infty = \alpha_m/(\alpha_m + \beta_m)$ and $\tau_m = 1/(\alpha_m + \beta_m)$, which may be more directly related to voltage-clamp measurements.

In several experimental studies, no effect on the kinetic behavior of T-type Ca^{2+} currents was observed when the intracellular Ca^{2+} concentration was varied, when extracellular Ca^{2+} was replaced by Ba^{2+} as the charge carrier, or under conditions where Ca^{2+} or Ba^{2+} accumulation could not occur (Carbone and Lux 1984, 1987a; Hernández-Cruz and Pape 1989; Nowycky et al. 1985). The inactivation gate of the T-type Ca^{2+} channel is therefore regarded as insensitive to the intracellular Ca^{2+} concentration. Using *Eq. 2* for m and a similar equation for h, Coulter et al. (1989) fit, according to a least-squares criterion, values for m_∞, h_∞, τ_m, and τ_h (and the cubic power for m) to their voltage clamp time courses of the T-type Ca^{2+} current. They provided analytic expressions for m_∞ and h_∞, but not for τ_m and τ_h.

Our model extends the above treatment in three ways. First, we note that the preceding description accounts for the inactivation on a moderately short time scale (<100 ms). It does not represent the slower component in the biphasic development of inactivation and the slow recovery from inactivation that have been reported for the T-type Ca^{2+} current (Bossu and Feltz 1986; Carbone and Lux 1984, 1987a; Coulter et al. 1989). To account for these effects, we consider a model for the inactivation gate that has two closed states (C_1 and C_2) and one open (O) state (Fig. 1B). Considerably lower transition rates into and out of the "deep" closed state C_2 provide the mechanism for the slower stage of inactivation. Defining h, s, and d as the fractions of inactivation gates in the states O, C_1, and C_2, respectively, the equations for h and d are

$$\dot{h} = \alpha_1(1 - h - d) - \beta_1 h \tag{3a}$$

$$\dot{d} = \beta_2(1 - h - d) - \alpha_2 d \tag{3b}$$

where we have made use of the relation $h + s + d \equiv 1$.

Second, by including a constant conductance leakage current, I_L, we formulate a two-current model for the membrane free from voltage control. Our current balance equation takes the form

$$C_m \dot{V} = -g_T m^3 h (V - V_{Ca}) - g_L (V - V_L) + I_{app} \tag{4}$$

where I_{app} ($\mu A/cm^2$) is the applied current. Values for the maximal conductances g_T and g_L lie in ranges that may be estimated for the acutely dissociated cell preparation. Assuming membrane area of ~1,000–2,000 μm^2, we can match the amplitude of I_T under voltage-clamp (range: 100–400 pA; Coulter et al. 1989; Suzuki and Rogawski 1989) with g_T = 0.1–0.6 mS/cm^2. In our model the leakage term dominates in setting a stable resting potential, V_{rest}. Under physiological conditions, several inward and outward currents contribute to establishing the rest state. However, the conductances of these currents are here presumed only weakly sensitive to voltage within the range relevant to I_T and to the LTS. Therefore, we consider I_L in *Eq. 4* as the summation of any such other currents with conductances that are relatively constant during the LTS. For dissociated relay neurons the input resistance varies over a range 0.3–2.0 GΩ (Suzuki and Rogawski 1989). Thus we choose g_L equal to 0.1 mS/cm^2 to be consistent with these data and the aforementioned membrane area. This value of g_L implies, for C_m = 1 $\mu F/cm^2$, a resting time constant of 10 ms. For all our simulations we set V_L = −65 mV, which typically leads to a value of V_{rest} around −63 mV. The system of *Eqs. 2–4* constitutes our minimal model, which generates an LTS and describes its slow recovery under current clamp conditions.

Finally, to perform computational experiments with our model, we need analytic expressions for the voltage-dependent kinetic rate functions. These also allow us to simulate physiological behav-

ior beyond the voltage range over which Coulter et al. (1989) determined τ_m and τ_h (−62 to −12 mV). We next describe our determination of these rate coefficients.

Activation gate

We adopt the steady-state activation function provided by Coulter et al. (1989)

$$m_\infty = \frac{1}{1 + \exp[-(V + V_s + 63)/7.8]} \quad (5)$$

where the parameter V_s is used to describe the effect of changing extracellular Ca^{2+} concentration, $[Ca^{2+}]_o$. For the baseline case, $[Ca^{2+}]_o$ = 3 mM, we set V_s = 0 mV.

To find an analytic expression for τ_m, we use the definition

$$\alpha_m^{-1} = \tau_m / m_\infty \quad (6)$$

and, by linear regression, we fit the experimental data [*Eq. 5* and values of τ_m from Fig. 5 of Coulter et al. (1989)] with an exponential function plus a constant (cf. Fig. 2A). The result is

$$\alpha_m = \frac{1}{1.7 + \exp[-(V + V_s + 28.8)/13.5]}. \quad (7)$$

It follows from *Eqs. 5–7* that

$$\tau_m = \frac{1.7 + \exp[-(V + V_s + 28.8)/13.5]}{1 + \exp[-(V + V_s + 63)/7.8]} \quad (8)$$

Inactivation gate

In our model there are four rate coefficients for the inactivation kinetics, α_1, β_1, α_2, and β_2, or equivalently

$$K_1 = \beta_1/\alpha_1 \quad K_2 = \beta_2/\alpha_2 \quad \tau_1 = 1/(\alpha_1 + \beta_1) \quad \tau_2 = 1/(\alpha_2 + \beta_2) \quad (9)$$

The steady-state inactivation function was estimated by Coulter et al. (1989) as follows

$$h_\infty = \frac{1}{1 + \exp[(V + V_s + 83.5)/6.3]}. \quad (10)$$

We examined several possible approaches to determining the two equilibrium functions K_1 and K_2 from h_∞. We noted that if K_2 is independent of voltage, it was not possible to account adequately for the recovery of I_T. This can be understood by observing that, according to *Eq. 3b*, K_2 equals the occupation of the deep closed state C_2 relative to that of C_1 at equilibrium. In the voltage-clamp recovery experiment of Coulter et al. (1989), it was found that, on the one hand, a brief hyperpolarization from a more depolarized level led to a minor initial recovery. Thus at a depolarized level the occupation in the deep closed state C_2 should be high, and K_2 should be large, so that during a short hyperpolarization the amount of flux to the open state O is limited by the small fraction available in the C_1 state. On the other hand, the complete recovery at a longer time scale requires that on persistent hyperpolarization the occupation in C_2 ought to be low, and K_2 should have a smaller value. Both requirements could not be satisfied with a fixed value of K_2. Therefore K_2 must be voltage dependent. We settled on the simplifying assumption that the two transition steps in Fig. 1B have similar equilibrium properties, albeit with very different time constants: $K_1 = K_2 \equiv K$. This convenient approximation will be justified a posteriori by the agreement between the resulting model simulations and experimental observations. It now follows from the steady-state solution of *Eq. 3* and from *Eq. 10* (see APPENDIX for details) that

$$K = \sqrt{0.25 + \exp[(V + V_s + 83.5)/6.3]} - 0.5 \quad (11)$$

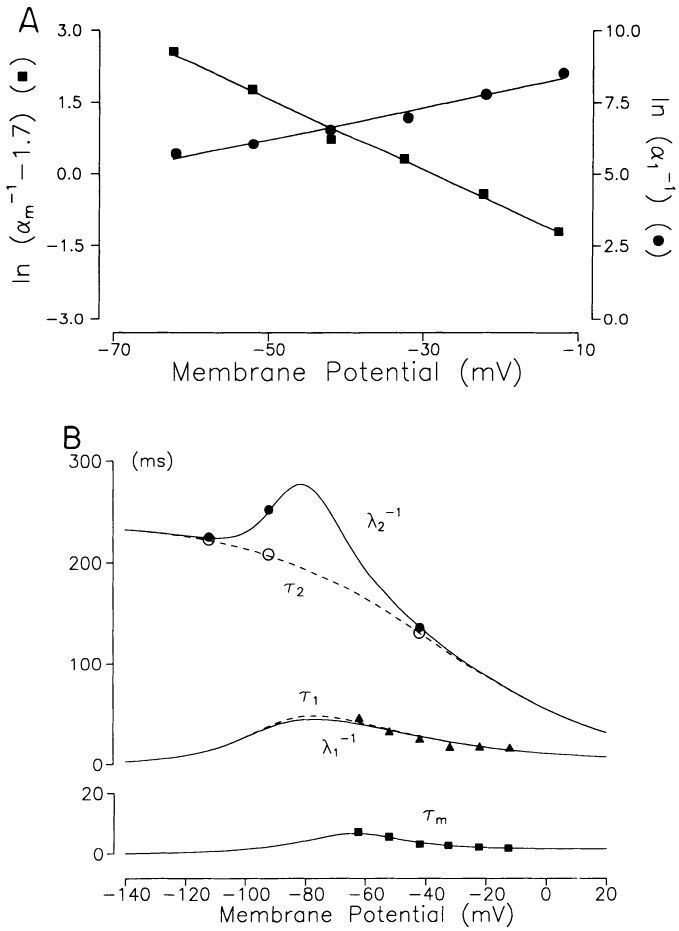

FIG. 2. Activation and inactivation time constants of the T-type Ca^{2+} channel. *A*: Coulter et al. (1989) provided 6 data points for $\tau_m(V)$ along with an expression for $m_\infty(V)$. This yields 6 values for $\alpha_m(V)$, according to *Eq. 6*, which were plotted as log $[\alpha_m(V)^{-1} - C]$ vs. V. The constant C was adjusted to the value 1.7 so that a straight line could be fit by linear regression, which led to the analytic expression for $\alpha_m(V)$ in *Eq. 7*. We obtain *Eq. 14* for the inactivation gating rate $\alpha_1(V)$ in a similar way (see text). *B*: filled circles indicate the experimentally measured values for τ_m, τ_h, and τ_r. Latter 2 are associated with the decay rates, λ_1 and λ_2, for *Eq. 3*. Kinetic time constant functions $\tau_1(V)$ and $\tau_2(V)$, given in terms of λ_1 and λ_2 by *Eq. A7* (see text and APPENDIX), are plotted here with dashed curves (and open circles in the case of τ_2). Solid curves (*top*) are according to *Eq. A6*. Solid curve for τ_m (*bottom*) is from *Eq. 8*. These data correspond to room temperature.

It remains to determine τ_1 and τ_2 or, equivalently, α_1 and α_2. Recall that Coulter et al. (1989, Fig. 5) described inactivation kinetics with a single τ_h. Their estimations were based on voltage-clamp data over a restricted time scale, 60–100 ms, which is relatively short compared with a typical recovery time from inactivation (≈250 ms). In addition, they as well as Suzuki and Rogawski (1989) measured a slow time constant, τ_r, for the recovery process at a few voltage values. To represent these disparate time scales in our two-step model of inactivation, it seems plausible to associate τ_h with the time constant of the faster transition step between the states O and C_1 in the scheme of Fig. 1*B* and to attribute the recovery time constant τ_r to the slow step between the states C_1 and C_2. However, the correspondence is not immediate. Although the faster time constant is likely unaffected by the slower transition process and thus is identifiable with τ_1, the recovery time constant certainly depends on both slow and fast processes (hence on τ_2 and τ_1).

The mathematically exact time constants of our model of the three-state inactivation gate are λ_1^{-1} and λ_2^{-1} where λ_1 and λ_2 are the

characteristic decay rates of the system *Eq. 3, a* and *b*. These time constants correspond to the measurable quantities τ_h and τ_r, respectively. In the APPENDIX we show how $\lambda_{1,2}$ are related to $\tau_{1,2}$ through a quadratic formula, and we use this to show that

$$\tau_1 \approx \lambda_1^{-1} = \tau_h \tag{12}$$

With this approximation we can substitute for τ_1 the experimental values for τ_h and evaluate the right side of

$$\alpha_1^{-1} = \tau_1[1 + K] \tag{13}$$

which follows from *Eq. 9*. Thereby we can obtain, as we did by linear regression for α_m above, an exponential function for α_1 (cf. Fig. 2*A*)

$$\alpha_1 = \exp[-(V + V_s + 160.3)/17.8] \tag{14}$$

According to the definition in *Eq. 9*, multiplying this by K yields an analytic expression for β_1 (not shown here). Then τ_1 follows from *Eq. 13*, and it has a maximum of ~45 ms near $V = -85$ mV (Fig. 2*B*).

Relatively few measurements are available for estimating the long time constant of *Eq. 3*. From the recovery experiments of Coulter et al. (1989, Fig. 7), we have $\lambda_2^{-1} \approx 220$ and 243 ms at −112 and −92 mV, respectively. An additional datum for λ_2^{-1} (at $V = -42$ mV) was obtained by fitting a sum of two exponentials to the decay of the uninterrupted I_T transient in their Fig. 7; the time constant estimated for the slower phase is 135 ms. These values are plotted in Fig. 2B (filled circles) together with the corresponding values of τ_2 (open circles) as given by *Eq. A7*. A simple form for τ_2 that is consistent with these measurements (decaying at depolarizing voltage and saturating in the other direction) is the sigmoid function

$$\tau_2 = \frac{240}{1 + \exp[(V + V_s + 37.4)/30]} \tag{15}$$

From this expression and *Eqs. 9* and *11* we get formulas for α_2 and β_2. The graph of τ_2 is shown in Fig. 2B where it may be compared with the recovery time constant, plotted as λ_2^{-1} versus V.

Temperature correction

The time constants above correspond to room temperature (22–24°C), at which the voltage-clamp experiments and our simulations thereof were performed. For our current-clamp simulations, we adjust the rates for "body temperature" (taken here to be 10°C greater than the preceding conditions). These results may then be compared with in vivo recordings or data obtained in slice preparations such as those reported by Thompson (1988), which were carried out at 34–35°C. To correct for temperature we use Q_{10} values of 5 and 3 for activation and inactivation (both steps), respectively (see Coulter et al. 1989). Thus, at body temperature, τ_m is multiplied by a factor of 0.2 and τ_1 and τ_2 by 0.33.

Numerical methods

Our numerical simulations have been carried out using the software package "PHASE PLANE" (Ermentrout 1990) for solving interactively differential equations on an IBM PC-compatible microcomputer. For the most part, we chose the Gear integration method to ensure a stable and accurate numerical solution for equations having the property of stiffness (i.e., disparate time scales). However, we found accurate computation did not require severe error control. For instance, satisfactory results were obtained with the Gear tolerance parameter set from 0.001 to 0.09 and maximum step size (in this variable step algorithm) set to 1.0 ms. We found that a comparable accuracy could be achieved using the fourth-order Runge-Kutta method with a fixed time step of 0.5 ms.

RESULTS

T-type Ca^{2+} current under voltage-clamp

Coulter et al. (1989) found that recordings of the T-type Ca^{2+} current during the initial 100 ms or so after a depolarizing voltage step could be fit accurately by the use of *Eq. 1* for I_T. Our extension of the model, intended to account for the slow recovery behavior, still accurately reproduces the early phase of the current. The time courses in Fig. 3A illustrate that, when the membrane is stepped from a relatively negative holding potential (−92 mV) to a more depolarized test potential (−42 mV), the deinactivated Ca^{2+} channels open and generate a transient current I_T [compare the *top panel* with Fig. 6, *A* and *B*, in Coulter et al. (1989)]. In the *bottom panel*, one sees a very rapid rise in activation followed by the early phase of inactivation as h decays on a time scale of tens of milliseconds. After 150 ms nearly all the inactivation gates have shifted from the open state O to the closed states C_1 and C_2. The gradual rise of d reflects the much slower kinetic step between C_1 and C_2. In spite of the fact that d has reached nearly 0.7 (tending toward its equilibrium level $d_\infty = 0.96$ at −42 mV), the transients of I_T, m, and h in Fig. 3A would change very little if the deep closed state C_2 were disallowed (by fixing $d = 0$). The slight differences are detectable only after ~100 ms.

The amplitude of I_T has been matched to the experimental data by our choice of $g_T = 0.4$ mS/cm^2. We note that, if the conductance of a single open T-type channel is assumed to be 8 pS (Carbone and Lux 1987b; Fisher et al. 1990; Fox et al. 1987b), this value for g_T implies that such an acutely dissociated relay cell has ~500–1,000 T-type Ca^{2+} channels.

Recovery of I_T from inactivation

Although the biphasic nature of inactivation is not apparent in Fig. 3*A*, it becomes so when a second I_T response is provoked, as in Fig. 3*B*. Because of the slow kinetics for d, a 50-ms return step to the holding potential allows only a minor decrease in d and therefore the channel deinactivates only slightly (h rises from 0 to ~0.2). The current I_T for the second depolarization to −42 mV shows little recovery, the ratio of the two I_T peaks being 0.28. In contrast, if C_2 were absent, and the kinetics of other steps were unchanged, then the second I_T peak would exceed 75% of the first one.

The time scale of transitions between C_1 and C_2 determines the relative refractory period of I_T. To quantitate the dynamics of recovery from inactivation, we have simulated a series of two-step runs in which the latency to the second test step (i.e., the duration of the holding pulse) is varied (Fig. 4*A*). As the latency increases beyond the slower time scale of inactivation, substantial recovery of I_T is achieved. If we seek to approximate this process with a single exponential (Fig. 4*B*), we obtain by linear regression a time constant of 237 ms. Our analytic expression (*Eq. A6*) for the slow time constant λ_2^{-1} at −92 mV yields 249 ms, and the approximation formula, *Eq. A9*, provides an excellent esti-

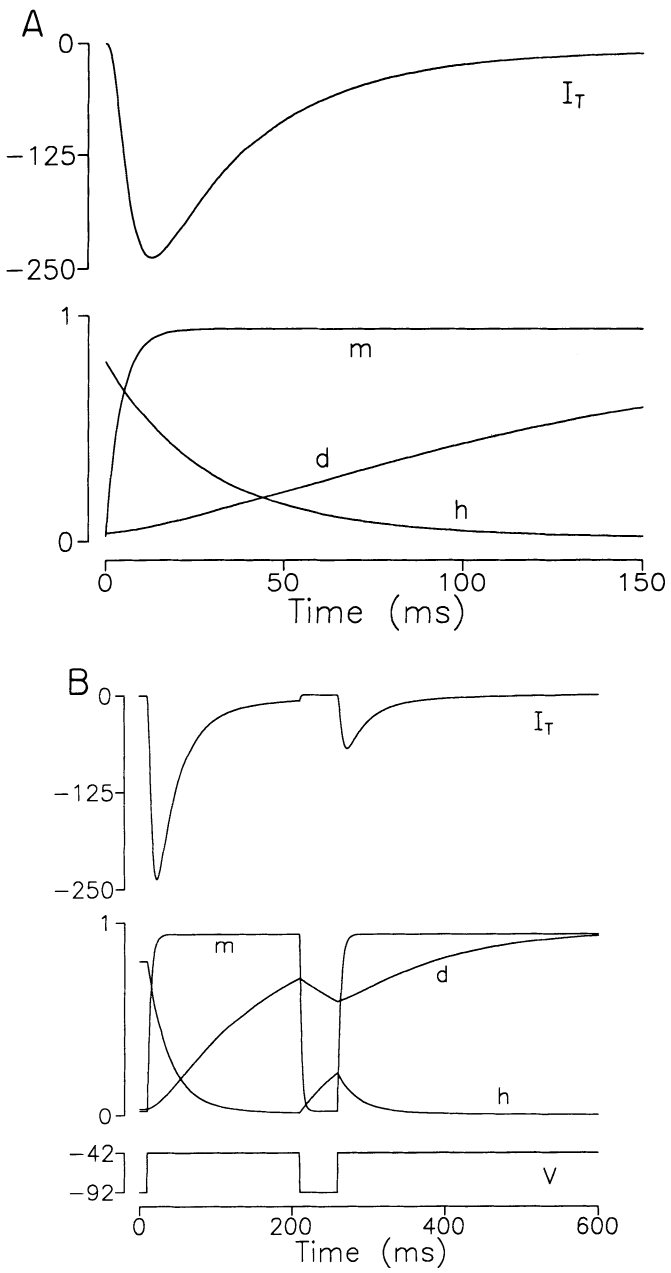

FIG. 3. *A*: time course of the T-type Ca^{2+} current (I_T) elicited by a voltage step from a holding potential (V_h) of −92 mV to a final potential of −42 mV as modeled with *Eqs. 1–3*. *Top*: I_T rises rapidly to a peak of −235 pA and decays in 2 phases (the late slower phase is less apparent than the fast early decay). *Bottom*: time courses of the channel variables $m(t)$, $h(t)$, and $d(t)$ corresponding to the current shown above. Slow change of $d(t)$ is responsible for the late decay phase of I_T. Here, we assume the thalamic relay neuron has a membrane area of 1,000 μm^2 corresponding to g_T = 0.4 mS/cm^2. *B*: partial recovery from inactivation of I_T in a simulated 2-pulse experiment. *Top*: the initial I_T response is elicited by a 200-ms step from −92 to −42 mV followed by a 2nd step with a delay of 50 ms. Only a fraction of I_T is recovered (ratio of the 2 peak current values is 0.28). *Bottom*: dependence of recovery on the time courses of $h(t)$ and $d(t)$. At start of the 2nd pulse, most of the inactivation gates are in the deep closed state C_2 and only a few reenter the open state O during the 50-ms repolarization.

mate, 242 ms, for this exact result. The modest discrepancies between these values and the simulation results are due to the limited range of recovery times (<450 ms) considered in Fig. 4*B*. These theoretical results on recovery compare well with the corresponding experimental data of Coulter et al. (1989) (see their Fig. 7, and with their estimate τ_r = 243 ms).

Our model is based primarily on experimental data from rat cells (Coulter et al. 1989), but we have also applied the model to mimic a set of recovery experiments carried out by Suzuki and Rogawski (1989), who used enzymatically isolated thalamocortical relay neurons from the guinea pig. These simulations required a change of the value of V_s in the model, because $[Ca^{2+}]_o$ = 10 mM was used instead of 3 mM in the latter experiments. Following an empirical rule of thumb (Frankenhaeuser and Hodgkin 1957), we shifted the voltage dependence of the gating kinetic rates positively by V_s = −10 mV for this approximately threefold increase in $[Ca^{2+}]_o$. A corresponding adjustment in the reversal potential V_{Ca}, using the Nernst expression, would have little effect on I_T and is disregarded here. Again we find close agreement between the theoretical and experimental results (Fig. 4*B*): the recovery time constant is 290 ms from the experiments, 278 ms from our simulations, and 256 and 246 ms from the analytical predictions (*Eqs. A6* and *A9*, respectively).

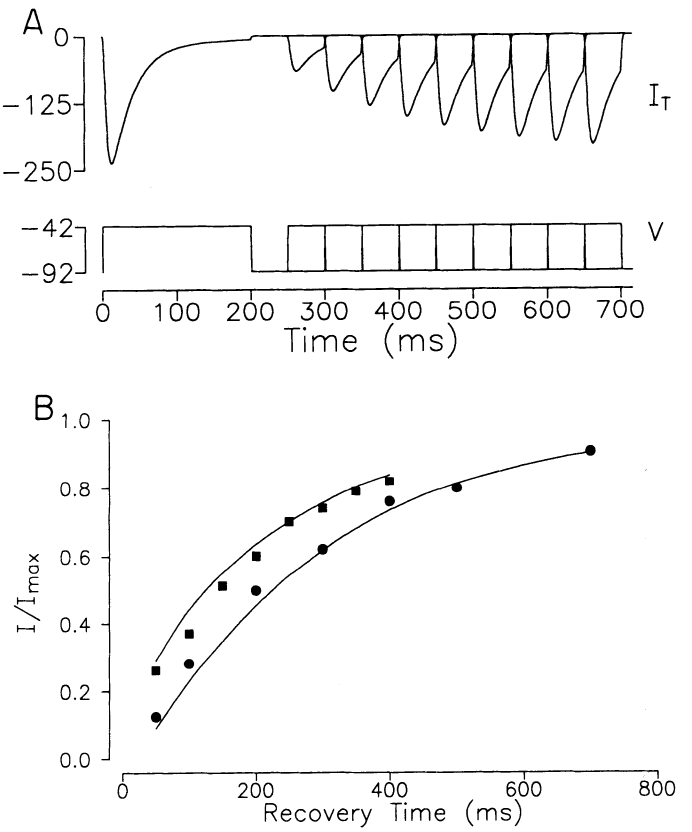

FIG. 4. *A*: increase in recovery of I_T as a function of the interpulse interval in a simulated 2-pulse experiment. Conditions are as in Fig. 3*B*. *B*: fractional recovery of I_T plotted vs. latency. Solid curves are best single exponential fits to the calculated values that allow an estimate of the theoretical recovery time constants. Squares indicate experimental data from Coulter et al. (1989); circles are from Suzuki and Rogawski (1989). Conditions in the former case are as in Fig. 3*B* ($[Ca^{2+}]_o$ = 3 mM); the recovery time constant τ_r equals 243 ms (experimental) or 237 ms (theoretical). In the latter case, the simulation was carried out assuming $[Ca^{2+}]_o$ = 9 mM and a holding potential of −80 mV; τ_r = 290 ms (experimental) and 278 ms (theoretical).

Low-threshold spike

To simulate current-clamp behavior we must integrate the full model, *Eqs. 2–4*. For these computations we use values of g_T in the range 0.1–0.6 mS/cm^2, and we adjust the kinetic rates for body temperature (see METHODS). Figure 5 shows an LTS as computed with our model after release from a hyperpolarized level of −92 mV. The resulting voltage trajectory has the characteristic triangular-shaped waveform of the LTS in recordings from brain slices and isolated neurons (Jahnsen and Llinás 1984a; Suzuki and Rogawski 1989). The initial voltage increase is due to the leakage current, which tends to drive V toward V_L. Indeed, the rising V slows as it nears V_L but then V continues to grow as the deinactivated I_T begins to increase. Notice (Fig. 5, *bottom*) that, at ~20 ms, although m is near its resting level (i.e., value at infinite time), h is large in comparison with its resting value, so that there is a net depolarizing current. The self-accelerating interaction between V and m leads to a transient spike, which is then counterbalanced by the inactivation process (decline in h). The peak of V occurs at ~30 ms, after the rapid drop of h to <20% of its initial value. The LTS decay is biphasic: the slower phase is evidenced here by the gradual relaxation of d, m, and V toward their rest values. It is interesting to note that, although h and the Ca^{2+} conductance $g_T m^3 h$ are small, repolarization of V does not proceed with the passive membrane time constant (10 ms). Because I_T has a large driving force, this current remains comparable in magnitude with the leakage current, and hence the return to rest is dominated first by the decay rate of h and subsequently by the decay of d.

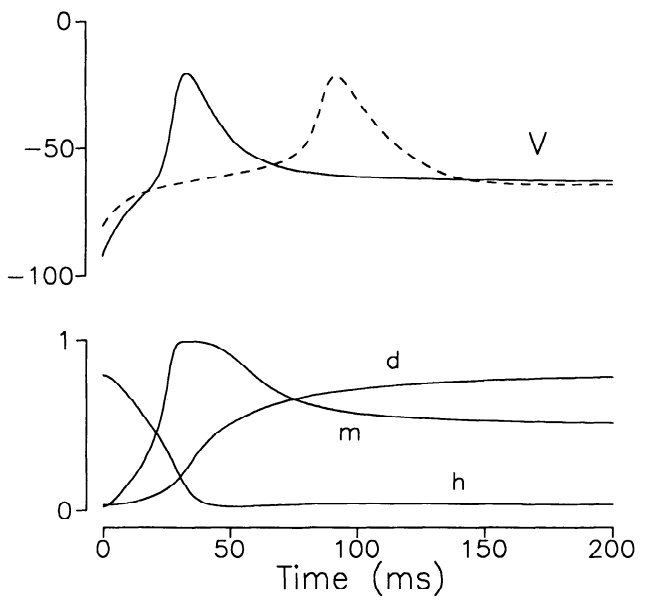

FIG. 5. Current-clamp simulation with only 2 membrane currents, I_T, and a constant conductance leakage current. Model generates a low-threshold spike (LTS) on release from hyperpolarization at *time 0*. Time courses of membrane potential (*top*) and gating variables (*bottom*) obtained by numerical integration of *Eqs. 2–4*. Here and in subsequent figures, g_L = 0.1 mS/cm^2, V_L = −65 mV, and kinetic rates are adjusted for body temperature. Early repolarization of the LTS is associated with a rapid drop of h to near 0, whereas the later stage in the return of V to the resting level (−63 mV) reflects the slow phase of inactivation, i.e., the gradual rise of d. Solid curves are for $[Ca^{2+}]_o$ = 3 mM, V_h = −92 mV, and g_T = 0.25 mS/cm^2. Dashed curve (*top*) illustrates prolonged plateau before upstroke of LTS under altered parameter conditions corresponding to an elevation of $[Ca^{2+}]_o$ to 9 mM (V_h = −80 mV; g_T = 0.52 mS/cm^2). At this higher $[Ca^{2+}]_o$ level, the voltage dependence of the channel kinetic rate constants are shifted in a positive direction (V_s = −10 mV). With these parameters, V hovers longer near the resting level after the release from hyperpolarization because the growth rate of m is diminished in this voltage range; finally m increases sufficiently to induce an LTS.

The initial depolarization that precedes the LTS exhibits, in some experiments, a more pronounced slowing of the voltage trajectory near V_L, resulting in a "plateau" before the firing of the LTS [Jahnsen and Llinás 1984a (Fig. 7); S. Suzuki and M. A. Rogawski, unpublished observations]. This plateau can be reproduced with our model on adjustment of various combinations of parameters as, for example, would occur with increased $[Ca^{2+}]_o$ (as used in the experiments of Suzuki and Rogawski 1989). The simulated voltage tracing under these conditions is shown by the dashed line in Fig. 5. To understand the delay in this case, recall that the voltage-dependent channel parameters are shifted to more positive voltages by higher $[Ca^{2+}]_o$. Thus, as V hovers near V_L, both m and its growth rate are smaller than in the preceding case and a longer time is needed for $m(t)$, hence $V(t)$, to grow. We emphasize, however, that the prolonged plateau does not necessarily require unphysiologically high Ca^{2+} levels. Indeed, significant delays can also be obtained with other parameter variations, such as decreasing V_L by 7–12 mV and simultaneously increasing g_T by a factor of 2–3. Such differences in parameter values could easily occur with variations in cell properties without a change in the intrinsic gating behavior of the T-type Ca^{2+} channel.

An important factor in shaping the LTS is the rate of inactivation compared with the time scale of $V(t)$ and $m(t)$. For example, if α_1 and β_1 were doubled, the LTS amplitude (solid curve, Fig. 5, *top*) would be reduced from about −21 to −45 mV. Corresponding sensitivity was also found if the transitions between O and C_1 were much slower: halving the rates would lead to a peak value of about +3 mV. In contrast, the kinetics of m are already quite fast, so that speeding the rates by a factor of 2 increases the LTS peak only to −17 mV. It appears that the h kinetics are well tuned to provide the proper time course of calcium conductance for LTS generation with g_T in our chosen range of values. Of course, if our model had additional outward currents, then offsetting adjustments could buffer such sensitivity.

Whereas the faster inactivation process affects the LTS waveform, the slow step of inactivation sets the minimum duration of hyperpolarization necessary to deinactivate I_T. Figure 6 shows how the response peak increases with duration: >100 ms of hyperpolarizing current is necessary to generate an LTS of greater than half-amplitude. The effect here is equivalent to that seen in the recovery experiments of Jahnsen and Llinás (1984a; see Figs. 6 and 7), and in our simulations of I_T recovery under voltage-clamp conditions (cf. Fig. 4*A*). If, at the beginning of hyperpolarization, a sizable fraction of inactivation gates are in the deep closed state C_2 (as at rest), then it will take an amount of time $\approx \tau_2$ for these channels to drift back to O, i.e., to deinactivate.

The LTS amplitude also varies with intensity of the hyperpolarization. In Fig. 7*A*, 200-ms current steps to various levels of hyperpolarization lead to a family of graded LTSs. The LTS amplitude saturates at strong hyperpolarizations

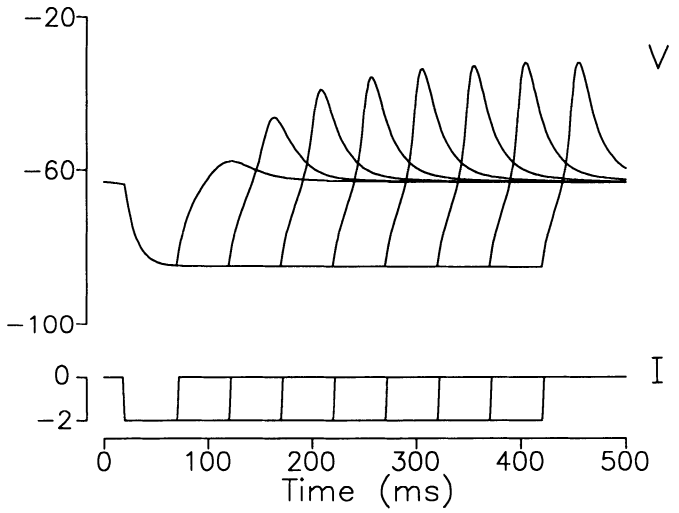

FIG. 6. Current-clamp simulations of the LTS evoked by hyperpolarizing current steps showing that the LTS amplitude increases with the duration of the hyperpolarization. Current step begins at t = 20 ms and continues for varying durations up to 400 ms (I_{app} = $-2\mu A/cm^2$). LTS exceeds 80% of its maximum amplitude for steps longer than 100 ms. g_T = 0.2 mS/cm^2, $[Ca^{2+}]_o$ = 3 mM.

because in this limit h attains its maximum value of 1. The response curve in Fig. 7*B* displays a sigmoid form and may be compared with the corresponding experimental data of Jahnsen and Llinás obtained over a more limited range (1984a, Fig. 4). Although there is not a strict threshold at these parameter settings (Fig. 7*B*), the behavior could be steeper with minimal adjustment in the parameters so as to simulate an "all or none" type of response pattern. For example, with increased $[Ca^{2+}]_o$ the computed peak of $V(t)$ shows a much sharper increase with stimulus strength (not shown). Similar phenomena have been seen experimentally in the presence of high $[Ca^{2+}]_o$ (Suzuki and Rogawski 1989).

Oscillatory behavior involving the LTS

If the LTS is critical to the generation of the 8- to 10-Hz rhythmic firing of thalamic relay neurons, it must be possible to evoke the LTS at the required frequency within the appropriate voltage domain. In an attempt to explore this issue, we consider the response of our minimal model to repetitive hyperpolarizing current stimulation. The case shown in Fig. 8*A* allows us to define our protocol. A full cycle of period P_o (ms) consists of hyperpolarization, I_{app} = -2.0 $\mu A/cm^2$, for p ms and then zero current for the remainder of the cycle. After each release an LTS is generated. In the example shown here, the driving frequency of 5 Hz is sufficiently low and p is long enough so that LTSs of constant amplitude are reliably evoked after each stimulus during the train.

The dependence of LTS amplitude on the frequency and pulse duration for such trains of hyperpolarizing pulses is summarized in Fig. 8*B*. To display the results on a single scale, we plot the adapted peak voltage versus p/P_o, the fraction of hyperpolarization per cycle. Indeed, as one expects, the response amplitude increases with the period of the stimulus, approaching saturation for periods longer than ~300 ms. Most striking, however, is the sensitivity seen for frequencies in the 5- to 10-Hz range. Here, the LTS amplitude for a range of hyperpolarization durations is adequate for generating a burst of spikes (i.e., the peak reaches threshold for Na^+-dependent action potentials; Suzuki and Rogawski 1989). If the stimulus is faster than ~12 Hz, the peak depolarization (for any fraction p/P_o) does not exceed −55 mV and drops dramatically for higher stimulus rates. For a fixed period, the LTS amplitude is graded with increasing duration of the hyperpolarizing pulse (corresponding to Fig. 6); it reaches −45 mV when p is ~100 ms (for $P_o \geq 200$ ms). The response is maximal for a duration larger than one-half of the total period, and then it decreases sharply when the release phase of the stimulus cycle is too brief (~30 ms). Although the quantitative details are affected, the qualitative aspects of Fig. 8 are preserved for variations in the amplitude and time course of the stimulating current. For example, if the hyperpolarizing pulse were -3.0 $\mu A/cm^2$ or if g_T = 0.3 nS/cm^2, the maximal response for P_o = 100 ms would be −30 and −35 mV, respectively, instead of −50 mV. Also, it is not essential that the applied hyperpolarization terminate abruptly. In fact, inhibitory postsynaptic

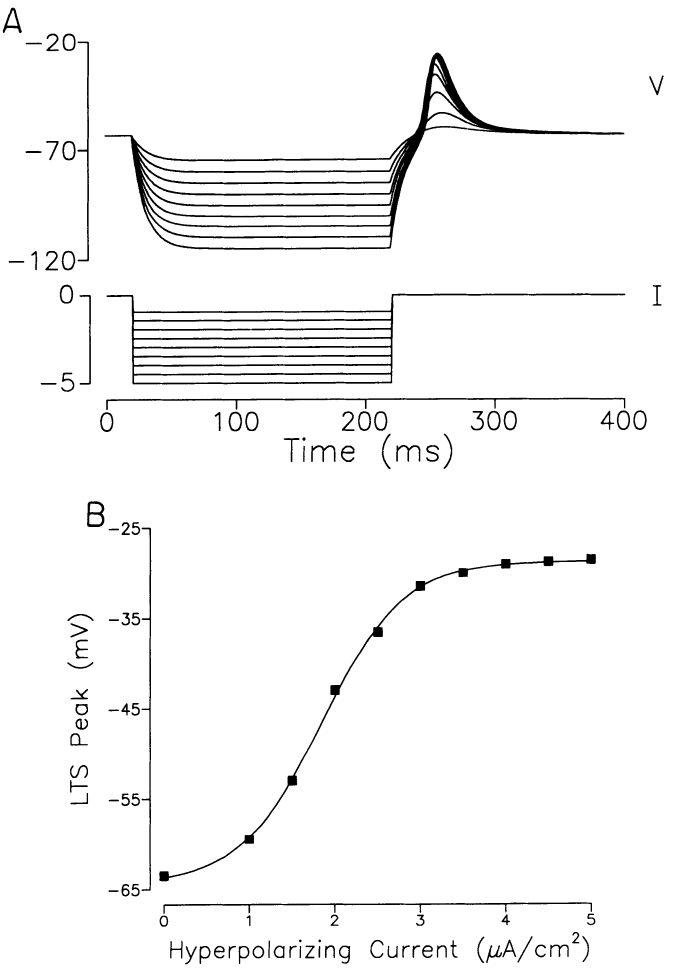

FIG. 7. Current-clamp simulations showing how the LTS amplitude increases with the intensity of the hyperpolarizing stimulus. *A*: family of LTSs evoked by 200-ms hyperpolarizing steps increasing in magnitude from −1 to −5 $\mu A/cm^2$ (g_T = 0.2 mS/cm^2). *B*: peak amplitude of the LTS plotted vs. the magnitude of the applied current step.

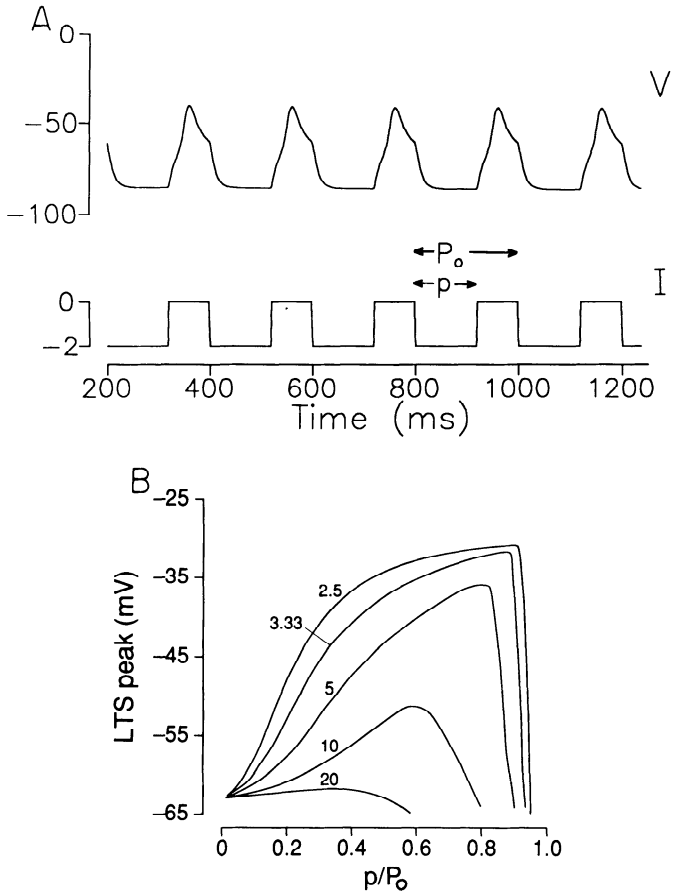

FIG. 8. Response of the model to a repetitive train of hyperpolarizing current pulses. Repetition period of stimulus is P_o and the step duration is p. $I_{app} = -2\mu mA/cm^2$ and $g_T = 0.25$ mS/cm^2. *A*: time course of membrane potential for $P_o = 200$ ms and $p = 120$ ms (5-Hz stimulus). After a single larger amplitude response at the start of the train (not shown), the LTS amplitude adapts rapidly to a constant amplitude. *B*: LTS amplitude (adapted) vs. p/P_o. Curves are for different stimulus periods ($P_o = 50$, 100, 200, 300, or 400 ms) and are labeled with the corresponding frequencies in Hz. Salient features: *1*) the LTS response is significantly attenuated if stimulus frequency exceeds 10 Hz; *2*) response saturates for frequencies <3 Hz; *3*) for a given P_o, the LTS amplitude first increases with the duration of the hyperpolarization (as described in Fig. 6) but then falls suddenly as the off-time of the stimulus, $P_o - p$, becomes shorter than the rise time of the full-amplitude LTS.

potentials (IPSPs) observed in thalamic neurons exhibit rather smooth decays (Thompson 1988). Computations with our model, in which I_{app} has an exponential decay phase, yield results similar to those above (not shown).

DISCUSSION

T-type Ca^{2+} current and the LTS

We have presented a theoretical model of the T-type Ca^{2+} channel based on kinetic parameters derived from recent voltage-clamp recordings using enzymatically isolated thalamic relay neurons. By virtue of the isolation procedure, these cells are electrically compact, allowing excellent spatial voltage control and accurate determination of kinetic parameters (Kay and Wong 1987). Although the T-type Ca^{2+} channel shares certain kinetic characteristics with the voltage-dependent Na^+ channel of fast action potentials (Hodgkin and Huxley 1952), an important difference between the two is that inactivation of the T-type Ca^{2+} channel occurs in two phases, the second of which is much slower than the first. To describe this characteristic of I_T, we proposed a kinetic scheme of the inactivation gate with two transition steps that possess disparate time constants. The slow outlet from the deep closed state is shown to serve as a "bottleneck" of the deinactivation process and controls its time course.

We studied the behavior of our model of the T-type Ca^{2+} current under simulated current-clamp conditions in an idealized cell endowed only with Ca^{2+} channels and a leakage pathway. Calculated current and voltage trajectories based on the model compare well with the experimental data and in particular provide insight into the long recovery time for the T-type Ca^{2+} current and the LTS. Thus there is a close correspondence between the recovery of the current in a simulated two-pulse experiment (Fig. 4*A*) and the actual experimental data obtained in two independent experiments (Fig. 4*B*). Moreover, in current-clamp simulations, we find that the shape (Fig. 5) and recovery (Fig. 6) of the LTS closely match results obtained in recordings from enzymatically isolated thalamic neurons (Suzuki and Rogawski 1989) as well as those obtained from relay neurons in thalamic slices (Crunelli et al. 1989; Jahnsen and Llinás 1984a,b; Llinás and Jahnsen 1982; Thompson 1988). The model allows sufficient flexibility to account for certain experimentally observed variations in cellular responsiveness, including the variable duration of the plateau phase that precedes the rapid upstroke of the LTS in current-clamp experiments (Fig. 5).

Our theoretical model of the T-type Ca^{2+} channel in thalamic relay neurons has several implications regarding the role of these channels in thalamic physiology and perhaps also in pathophysiological states, such as absence seizures. The demonstration that bursting in thalamic and other central neurons is mediated by Ca^{2+}-dependent low-threshold spikes (see Llinás 1988) along with the subsequent identification of transient low-threshold (T-type) Ca^{2+} channels in various neuronal and muscle cells (Carbone and Lux 1984; Hagiwara et al. 1988; Nilius et al. 1985; Nowycky et al. 1985) led naturally to the proposal that these channels play a role in the bursting behavior of some neurons (Miller 1987). Subsequent pharmacological studies have provided strong confirmatory evidence that T-type Ca^{2+} channels are critical to the generation of the LTS event, at least in thalamic neurons (Suzuki and Rogawski 1989; Thompson 1988). Nevertheless, it has remained unclear whether the intrinsic properties of these active elements alone are responsible for the main features of the LTS. Our model suggests that they are. Although other membrane currents may perhaps modify the likelihood with which a given synaptic stimulus elicits an LTS and undoubtedly play a role in subtly shaping the voltage trajectory of the LTS, the intrinsic properties of the T-type Ca^{2+} channel alone are sufficient to generate the main features of the LTS.

Limitations of the model

Despite its utility, our model of the thalamic relay neuron has certain limitations. First, it ignores the presence of other voltage- and Ca^{2+}-dependent currents, including the

transient K^+ current (I_A) (Rogawski 1985; Rudy 1988) and a hyperpolarization-activated cation current (I_h; McCormick and Pape 1990), that likely influence the cell's subthreshold behavior. Because our model is sufficient to reproduce the characteristic features of the LTS, we propose that these currents may alter the rate and pattern of repetitive bursting but are not critical to generating the burst other than in shaping fast Na^+-dependent action potentials. (Ionic currents associated with the Na^+ spike do not appear to play a major role in specifying the trajectory of the LTS because tetrodotoxin does not alter the LTS shape.) In fact, the voltage-dependent properties of the active K^+ currents in thalamic neurons are such that they would not be predicted to substantially alter the voltage trajectory of the LTS. Unlike the classical delayed rectifier K^+ current (I_K) of the squid giant axon (but similar to the current in some other central neurons; see, e.g., Ffrench-Mullen and Rogawski 1989), I_K in thalamic relay cells shows substantial activation only on depolarization to potentials more positive than about −20 mV (S. Suzuki and M. A. Rogawski, unpublished observations), a level that is not reached by the LTS. I_A is activated at somewhat more hyperpolarized levels; i.e., in thalamic neurons, the threshold is about −50 mV and one-half activation occurs at about −30 mV ($[Ca^{2+}]_o$ = 5 mM). The peak conductance of I_A in thalamic neurons is comparable with that of the T-type Ca^{2+} current. The current activates rapidly (<10 ms) and inactivates with a time constant of ~60–80 ms (at room temperature). Simulations of our model, which included an additional I_A with these experimentally determined parameters (with appropriate adjustment for normal $[Ca^{2+}]_o$ and body temperature), indicated that I_A caused at most a modest (<18%) reduction in the peak amplitude of the LTS with little effect on its shape. I_A in thalamic relay cells is one-half inactivated at about −75 mV. We tested the sensitivity of the computed LTS to the position along the voltage axis of this half-inactivation point and found that a shift in the depolarizing direction does not substantially alter the shape of the LTS, although its amplitude is further reduced (33% for +10 mV). We therefore conclude that neither of the major voltage-dependent K^+ currents is critical to specifying the voltage trajectory of the LTS, but these currents may modify the behavior of the cell during the interval between burst events and will certainly need to be taken into account in a complete model of the electroresponsiveness of the thalamic relay neuron. With regard to Ca^{2+}-activated K^+ channels, little information is available for thalamic neurons, and, in fact, slow Ca^{2+}-activated K^+ channels may not exist in these cells (see McCormick and Pape 1990), so that at present it is premature to speculate on the role these channels might play in determining the membrane potential behavior during bursting.

Another feature of the thalamic relay neuron that we did not consider is its morphological complexity and the possible presence of T-type Ca^{2+} channels on cellular processes as well as on the soma. In other neuronal cell types, Ca^{2+} channels have been localized to dendritic regions (Jones et al. 1989; Lipscombe et al. 1988; Llinás 1988; Llinás and Sugimori 1980; Tank et al. 1988; Westenbroek et al. 1990). The distribution of T-type Ca^{2+} channels has not yet been determined, although there is some evidence that these channels may be present in dendrites (Harris et al. 1989). In thalamic relay neurons, T-type Ca^{2+} channels are clearly present in the somatic or proximal dendritic membrane (Steriade et al. 1990; Suzuki and Rogawski 1989); however, the extent to which the channels are also present on distal dendrites is uncertain. Nevertheless, spatial segregation of Ca^{2+} channels to dendrites would complicate the interpretation of interactions between local synaptically driven dendritic potentials and the firing behavior of the soma that presumably determines the output properties of the cell. This problem is highlighted by the experimental observation of Thompson (1988) that IPSPs, which cause no change in membrane potential measured at the soma, are capable of evoking an LTS, presumably because they sufficiently hyperpolarize local regions of the dendritic membrane. Nevertheless, in general terms, our model of the LTS is as applicable to the local milieu of the dendrite as it is to the soma. However, if the LTS is generated locally in dendrites, it must presumably be transmitted to the soma to generate fast action potentials (Wollner and Catterall 1986).

Endogeneous oscillations in thalamocortical relay neurons

Although the 10-Hz spindling oscillation of relay neurons is believed to be crucially dependent on the phasic inhibition from the reticular nucleus, the T-type Ca^{2+} current, together with other ionic currents, might endow thalamic relay neurons with the capability of generating endogeneous bursting behaviors. In fact, a slower, 1- to 2-Hz bursting oscillation has been observed in both in vivo and in vitro recordings (Leresche et al. 1990; McCormick and Pape 1990). With the experimentally determined parameter values, our model does not display rhythmic behavior. McCormick and Pape (1990) have suggested that the 1- to 2-Hz oscillation can be accounted for by the combination of the T-type Ca^{2+} current and the hyperpolarization-activated cation current (I_h), which they characterized in their thalamic slice recordings. We found that inclusion of I_h enables our model to produce similar slow oscillations if we use the kinetic parameters for the h-type current provided by these authors; if the passive time constant C_m/g_L is increased to 50 ms, and if a strong steady hyperpolarizing current is applied (unpublished observations).

We also explored the conditions under which, without I_h, the parameter values in our model might be modified to produce self-sustained oscillations in the frequency range of 10 Hz. After examining a range of values for g_T and I_{app} without success, we found that rhythmicity occurs under either of the following two conditions. When m_∞ and h_∞ are translated along the voltage axis to bring their midpoints closer together than are observed experimentally, our model generates repetitive LTSs in response to a constant hyperpolarizing current (Fig. 9). Alternatively, autooscillatory activity occurs when the slow phase of inactivation is eliminated by setting $d = 0$.

Recently, Rose and Hindmarsh (1989) developed a different theoretical model of the thalamic relay cell that also supports endogenous oscillatory bursting. This model differs from the present one by utilizing a simpler functional form for the low-threshold Ca^{2+} current (I_s in their

notation) and by including several other currents. The Rose-Hindmarsh model was formulated before the availability of the recent voltage-clamp data on the T-type Ca^{2+} current in thalamic neurons, and it does not account for the slow recovery of the T-current. Thus the inactivation gate for I_s has two states and a single voltage-independent time constant (τ_{h_s} = 25 ms). The other currents in the model include a fast Na^+ current, I_{Na}; a noninactivating, delayed-rectifier K^+ current, I_K; a transient (inactivating) K^+ current, I_A; and a leakage current, I_L. In the subthreshold voltage range, I_{Na}, I_K, and I_A are small and not strongly voltage dependent. Consequently, they may be cast into an "effective" leakage current. Under such circumstances, this model predicts current-clamp behavior in response to applied current similar to that of our present model in the absence of the slow inactivation step ($d = 0$). Moreover, the additional currents in their complete model lead to spike generation when V passes threshold in response to a depolarizing stimulus. Under a constant hyperpolarizing current their model also exhibits repetitive LTS-driven bursting oscillations. Although this automatic firing mode is unlikely to be relevant to the in vivo behavior of thalamic relay neurons per se, it is conceivable that such rhythmic burst firing occurs in neurons of the nucleus reticularis thalami, which also possess T-type Ca^{2+} channels and which may be capable of oscillations (Mulle et al. 1986). In fact, it is believed that these latter neurons may drive the burst firing of relay neurons (Steriade et al. 1987). Similarly, our model could be applicable to the reticularis neurons if the T-type Ca^{2+} channels in these cells had the characteristics described above.

We are still at an early stage of identifying the relative contributions made by intrinsic cellular properties and by intercellular coupling in generating the rhythm. As additional biophysical data become available, we anticipate that theoretical models will be improved and will be used to gain further insight into the mechanisms that underlie these rhythms.

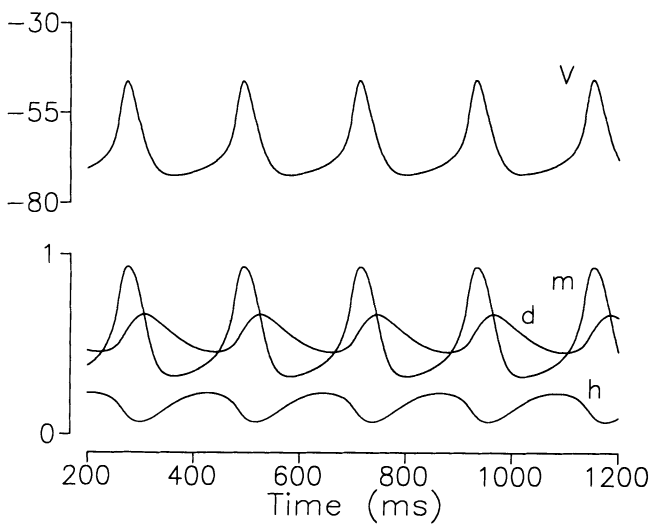

FIG. 9. LTS model exhibits intrinsic oscillations for altered parameter values. Modest translations of the voltage dependence of $m_\infty(V)$ and $h_\infty(V)$ cause them to overlap. In this example, the midpoint of $m_\infty(V)$ is shifted from −63 to −65 mV and that of $h_\infty(V)$ from −83.5 to −75 mV. With g_T = 0.2 mS/cm^2 and I_{app} = −1.0 μA/cm^2, the oscillation period is ~200 ms (body temperature).

Implications for thalamic spindling and absence seizures

Under ordinary conditions, burst firing of thalamic relay neurons occurs during slow-wave sleep and is associated with spindling in the cortical electroencephalogram (Steriade and Deschênes 1984). Electrophysiological recordings from thalamic relay neurons in vivo have indicated that burst firing during spindling is accompanied by a barrage of inhibitory potentials arising from neurons in the nearby nucleus reticularis thalami (Houser et al. 1980; Roy et al. 1984; Steriade et al. 1986). These inhibitory events deinactivate the T-type Ca^{2+} current so that an LTS and a burst of spikes is elicited as the membrane potential of the relay neuron recovers at the termination of the inhibitory drive. Such a scheme is supported by recordings from relay neurons in thalamic brain slices, which have demonstrated that trains of conventional IPSPs elicited by stimulation of the nucleus reticularis can result in the rebound excitation of an LTS without the intervention of any excitatory input (Thompson 1988). However, in these in vitro studies, the inhibitory drive needed to be maintained for >50–100 ms, and recordings in vivo have shown that the IPSPs typically have a duration of 60–120 ms. Consequently, in our current-clamp simulations we have investigated the voltage and time dependency for activation of the LTS by a hyperpolarizing stimulus. The LTS amplitude is seen to increase in a monotonic fashion with larger hyperpolarizing steps (Fig. 7), and this corresponds with the graded nature of the LTS recorded in brain slices (Thompson 1988). Moreover, it is apparent (Fig. 8) that the period of hyperpolarization required to evoke an LTS in our simulations is compatible with the IPSP duration in the in vitro recordings and the actual duration of the inhibition recorded under more physiological conditions in vivo. We note that the predictions of Fig. 8 are strikingly similar to the experimental observations of McCormick and Feeser (1990), displayed in a similar fashion in their Fig. 3.

During spindling, thalamic neurons exhibit bursting at a frequency of ~10 Hz. Does our theoretical model permit bursting to occur at this rate? In vivo recordings have indicated that the hyperpolarization level between bursts is −80 mV (see, e.g., Fig. 2*C* in Deschênes et al. 1984). The slow time constant of inactivation of the T-type Ca^{2+} current at −80 mV is 275 ms (measured at 25°C and with $[Ca^{2+}]_o$ = 3 mM). Using the Q_{10} of 3 determined by Coulter et al. (1989) to correct the time constant to body temperature (and also correcting for the in vivo Ca^{2+} concentration of 2.5 mM), we obtain an estimate for the in vivo inactivation time constant at −80 mV of 90 ms, which should allow the T-type Ca^{2+} current to be activated at a sufficient rate.

The thalamus has long been considered to be a critical structure in the generation of the spike-and-wave discharges recorded in the cortex during absence seizures. These stereotyped discharges occur at a frequency of 3 Hz in cats and humans; similar electroencephalographic events occur at 8–10 Hz in rodents with absence-like seizures (Vergnes et al. 1987, 1990). It has been argued that the activity of the thalamic neurons during the spike-wave dis-

charge is similar to that occurring during spindling (Gloor 1984). If so, the cells would fire in the bursting mode that is dependent on T-type Ca^{2+} channels. Our estimate of the upper limit for the frequency of burst firing in thalamic neurons is surprisingly close to the maximum spike-wave discharge frequency during absence seizures in rodents (10 Hz). Thus our results indicate that the thalamic neuron is competent to discharge in burst mode at either the cat and human or rodent frequencies.

APPENDIX

At fixed voltage, the steady state of *Eq. 3* determines the functions h_∞ and d_∞ for the inactivation variables h and d

$$\alpha_1(1 - h - d) = \beta_1 h \tag{A1a}$$

$$\beta_2(1 - h - d) = \alpha_2 d \tag{A1b}$$

Solving these equations in terms of the new parameters defined in *Eq. 9* yields

$$h_\infty = \frac{1}{1 + K_1[1 + K_2]} \tag{A2a}$$

$$d_\infty = K_1 K_2 h_\infty \tag{A2b}$$

The simplification $K_1 = K_2 \equiv K$ leads to

$$h_\infty = \frac{1}{1 + K + K^2} \tag{A3}$$

from which the expression for K, *Eq. 11*, follows.

The time courses of $h(t)$ and $d(t)$ are determined by solving the ordinary differential *Eqs. 3, a* and *b*, which are linear under voltage-clamp conditions. Each is a sum of two exponential terms

$$A_0 + A_1 \exp[-\lambda_1 t] + A_2 \exp[-\lambda_2 t] \tag{A4}$$

where $-\lambda_1$ and $-\lambda_2$ are the characteristic roots of this second-order system. They satisfy the quadratic equation

$$\lambda^2 + Tr \quad \lambda + D = 0 \tag{A5a}$$

where

$$Tr = -(\alpha_1 + \beta_1 + \alpha_2 + \beta_2) = -(1/\tau_1 + 1/\tau_2)$$

$$D = \alpha_1\alpha_2 + \beta_1(\alpha_2 + \beta_2) = \frac{1 + K(1 + K)}{\tau_1\tau_2(1 + K)^2} \tag{A5b}$$

Thus λ_1 and λ_2 are given by

$$\lambda_1, \lambda_2 = \frac{1}{2}\left\{(1/\tau_1 + 1/\tau_2) \pm \sqrt{\left(\frac{1}{\tau_1} - \frac{1}{\tau_2}\right)^2 + \frac{4K}{\tau_1\tau_2(1 + K)^2}}\right\} \tag{A6}$$

The directly measurable time constants in experiments are λ_1^{-1} and λ_2^{-1} (i.e., τ_h and τ_r, respectively) rather than τ_1 and τ_2. To get analytic expressions for the latter, we must express them in terms of λ_1 and λ_2. Therefore we invert *Eq. A6* to obtain

$$\tau_1^{-1}, \tau_2^{-1} = \frac{1}{2}\left\{(\lambda_1 + \lambda_2) \pm \sqrt{(\lambda_1 + \lambda_2)^2 - \frac{4(1 + K)^2\lambda_1\lambda_2}{1 + K(1 + K)}}\right\} \tag{A7}$$

A useful approximation for τ_1 may be obtained if we factor λ_1 out of the right side in *Eq. A7*. Now because the ratio λ_2/λ_1 is small (because $\tau_r \gg \tau_h$), we form a Taylor's series expansion and retain only the first term to arrive at

$$\tau_1 \approx \lambda_1^{-1} \tag{A8}$$

To approximate τ_2 we use the fact $\lambda_1\lambda_2 = D$ in *Eq. A5* and then eliminate λ_1 by using *Eq. A8* to obtain

$$\tau_2 \approx \lambda_2^{-1}[1 + K(1 + K)]/(1 + K)^2 \tag{A9}$$

This formula shows how one should adjust the measured τ_r to obtain τ_2; the factor involving K is between ¾ and 1.

We remark that *Eq. A9* may also be viewed as an approximation for the slow time constant λ_2^{-1} of *Eq. 3*, which can be obtained in a more direct way by exploiting the time scale differences in *Eq. 3*. That is, because *Eq. 3a* describes a much faster process than *Eq. 3b*, we use the rapid equilibrium hypothesis on the former: assume steady state, $dh/dt = 0$, and solve for h in terms of d. Substituting this into *Eq. 3b*, we obtain a single first-order equation for d, the decay rate of which approximates λ_2 and which, when rewritten using the definitions from *Eq. 9*, is equivalent to *Eq. A9*.

We thank Dr. Michael Weinstein for exploratory simulations with earlier versions of this model.

Address for reprint requests: X.-J. Wang, Mathematical Research Branch, NIDDK, NIH, Bldg. 31, Rm. 4B-54, Bethesda, MD 20892.

Received 21 December 1990; accepted in final form 19 April 1991.

REFERENCES

ANDERSEN, P. AND ANDERSSON, S. A. *Physiological Basis of the Alpha Rhythm.* New York: Appleton-Century-Crofts, 1968.

BOSSU, J.-L. AND FELTZ, A. Inactivation of the low-threshold transient calcium current in rat sensory neurones: evidence for a dual process. *J. Physiol. Lond.* 376: 341–357, 1986.

CARBONE, E. AND LUX, H. D. A low voltage-activated, fully inactivating Ca channel in vertebrate sensory neurons. *Nature Lond.* 310: 501–502, 1984.

CARBONE, E. AND LUX, H. D. Kinetics and selectivity of a low-voltage-activated calcium current in chick and rat sensory neurones. *J. Physiol. Lond.* 386: 547–570, 1987a.

CARBONE, E. AND LUX, H. D. Single low-voltage-activated calcium channels in chick and rat sensory neurones. *J. Physiol. Lond.* 386: 571–601, 1987b.

COULTER, D. A., HUGUENARD, J. R., AND PRINCE, D. A. Calcium currents in rat thalamocortical relay neurones: kinetic properties of the transient low-threshold current. *J. Physiol. Lond.* 414: 587–604, 1989.

CRUNELLI, V., LIGHTOWLER, S., AND POLLARD, C. E. A T-type Ca^{2+} current underlies low-threshold Ca^{2+} potentials in cells of the cat and rat lateral geniculate nucleus. *J. Physiol. Lond.* 413: 543–561, 1989.

DESCHÊNES, M., PARADIS, M., ROY, J. P., AND STERIADE, M. Electrophysiology of neurons of lateral thalamic nuclei in rat: resting properties and burst discharges. *J. Neurophysiol.* 51: 1196–1219, 1984.

ERMENTROUT, G. B. *PHASEPLANE: The Dynamical Systems Tool, Version 3.0.* Pacific Grove, CA: Brooks/Cole, 1990.

FFRENCH-MULLEN, J. M. H. AND ROGAWSKI, M. A. Interaction of phencyclidine with voltage-dependent potassium channels in cultured rat hippocampal neurons: comparison with block of the NMDA receptor-ionophore complex. *J. Neurosci.* 9: 4051–4061, 1989.

FISHER, R. E., GRAY, R., AND JOHNSTON, D. Properties and distribution of single voltage-gated calcium channels in adult hippocampal neurons. *J. Neurophysiol.* 64: 91–104, 1990.

FOX, A. P., NOWYCKY, M. C., AND TSIEN, R. W. Kinetic and pharmacological properties distinguish three types of calcium currents in chick sensory neurones. *J. Physiol. Lond.* 394: 149–172, 1987a.

FOX, A. P., NOWYCKY, M. C., AND TSIEN, R. W. Single-channel recordings of three types of calcium channels in chick sensory neurones. *J. Physiol. Lond.* 394: 173–200, 1987b.

FRANKENHAEUSER, B. AND HODGKIN, A. L. The action of calcium on the electrical properties of squid axons. *J. Physiol. Lond.* 137: 218–244, 1957.

GLOOR, P. Electrophysiology of generalized epilepsy. In: *Electrophysiology of Epilepsy,* edited by P. A. Schwartzkroin and H. V. Wheal. London: Academic, 1984, p. 109–136.

HAGIWARA, N., IRISAWA, H., AND KAMEYAMA, M. Contribution of two types of calcium currents to the pace-maker potentials of rabbit sino-atrial node cells. *J. Physiol. Lond.* 395: 233–253, 1988.

HARRIS, N. C., RAMSAY, S., KELION, A., AND GREENFIELD, S. A. Electrophysiological evidence for the dendritic localization of a calcium conductance in guinea-pig substantia nigra neurones in vitro. *Exp. Brain Res.* 74: 411–416, 1989.

HERNÁNDEZ-CRUZ, A. AND PAPE, H.-C. Identification of two calcium currents in acutely dissociated neurons from the rat lateral geniculate nucleus. *J. Neurophysiol.* 61: 1270–1283, 1989.

HODGKIN, A. L. AND HUXLEY, A. F. A quantitative description of membrane current and its application to conduction and excitation in nerve. *J. Physiol. Lond.* 117: 500–544, 1952.

HOUSER, C. R., VAUGHAN, J. E., BARBER, R. P., AND ROBERTS, E. GABA neurons are the major cell type of the nucleus reticularis thalami. *Brain Res.* 200: 341–354, 1980.

JAHNSEN, H. AND LLINÁS, R. R. Electrophysiological properties of guinea-pig thalamic neurones: an in vitro study. *J. Physiol. Lond.* 349: 205–226, 1984a.

JAHNSEN, H. AND LLINÁS, R. R. Ionic basis for the electroresponsiveness and oscillatory properties of guinea-pig thalamic neurones in vitro. *J. Physiol. Lond.* 349: 227–247, 1984b.

JONES, O. T., KUNZE, D. L., AND ANGELIDES, K. J. Localization and mobility of omega-conotoxin-sensitive Ca^{2+} channels in hippocampal CA1 neurons *Science Wash. DC* 244: 1189–1193, 1989.

KAY, A. R. AND WONG, R. K. Calcium current activation kinetics in isolated pyramidal neurones of the CA1 region of the mature guinea-pig hippocampus. *J. Physiol. Lond.* 392: 603–616, 1987.

LERESCHE, N., JASSIK-GERSCHENFELD, D., HABY, M., SOLTESZ, I., AND CRUNELLI, V. Spontaneous oscillations of cat and rat thalamocortical cells in vitro (Abstract). *J. Physiol. Lond.* 426: 45P, 1990.

LIPSCOMBE, D., MADISON, D. V., POENIE, M., REUTER, H., TSIEN, R. Y., AND TSIEN, R. W. Spatial distribution of calcium channels and cytosolic calcium transients in growth cones and cell bodies of sympathetic neurons. *Proc. Natl. Acad. Sci. USA* 85: 2398–2402, 1988.

LLINÁS, R. R. The intrinsic electrophysiological properties of mammalian neurons: insights into central nervous system function. *Science Wash. DC* 242: 1654–1664, 1988.

LLINÁS, R. R. AND JAHNSEN, H. Electrophysiology of mammalian thalamic neurones in vitro. *Nature Lond.* 297: 406–408, 1982.

LLINÁS, R. R. AND SUGIMORI, M. Electrophysiological properties of in vitro Purkinje cell dendrites in mammalian cerebellar slices. *J. Physiol. Lond.* 305: 197–213, 1980.

MCCORMICK, D. A. AND FEESER, H. R. Functional implications of burst firing and single spike activity in lateral geniculate relay neurons. *Neuroscience* 39: 103–113, 1990.

MCCORMICK, D. A. AND PAPE, H.-C. Properties of a hyperpolarization-activated cation current and its role in rhythmic oscillation in thalamic relay neurones. *J. Physiol. Lond.* 431: 291–318, 1990.

MILLER, R. J. Multiple calcium channels and neuronal function. *Science Wash. DC* 235: 46–52, 1987.

MULLE, C., MADARIAGA, A., AND DESCHÊNES, M. Morphology and electrophysiological properties of reticularis thalami neurons in cat: in vivo study of a thalamic pacemaker. *J. Neurosci.* 6: 2134–2145, 1986.

NILIUS, B., HESS, P., LANSMAN, J. B., AND TSIEN, R. W. A novel type of cardiac calcium channel in ventricular cells. *Nature Lond.* 316: 443–446, 1985.

NOWYCKY, M. C., FOX, A. P., AND TSIEN, R. W. Three types of neuronal calcium channel with different calcium agonist sensitivity. *Nature Lond.* 316: 440–443, 1985.

ROGAWSKI, M. A. The A-current: how ubiquitous a feature of excitable cells is it? *Trends Neurosci.* 8: 214–219, 1985.

ROSE, R. M. AND HINDMARSH, J. L. The assembly of ionic currents in a thalamic neuron. I–III. *Proc. R. Soc. Lond. B Biol. Sci.* 237: 267–334, 1989.

ROY, J. P., CLERCQ, M., STERIADE, M., AND DESCHÊNES, M. Electrophysiology of neurones of lateral thalamic nuclei in cat: mechanisms of long-lasting hyperpolarizations. *J. Neurophysiol.* 51: 1220–1235, 1984.

RUDY, B. Diversity and ubiquity of K channels. *Neuroscience* 25: 729–749, 1988.

STERIADE, M. AND DESCHÊNES, M. The thalamus as a neural oscillator. *Brain Res. Rev.* 8: 1–63, 1984.

STERIADE, M., DOMICH, L., AND OAKSON, G. Reticularis thalami neurons revisited: activity changes during shifts in states of vigilance. *J. Neurosci.* 6: 68–81, 1986.

STERIADE, M., DOMICH, L., OAKSON, G., AND DESCHÊNES, M. The deafferented reticular thalamic nucleus generates spindle rhythmicity. *J. Neurophysiol.* 57: 260–273, 1987.

STERIADE, M., JONES, E. G., AND LLINÁS, R. R. *Thalamic Oscillations and Signaling.* New York: Wiley, 1990.

SUZUKI, S. AND ROGAWSKI, M. A. T-type calcium channels mediate the transition between tonic and phasic firing in thalamic neurones. *Proc. Natl. Acad. Sci. USA* 86: 7228–7232, 1989.

TANK, D. W., SUGIMORI, M., CONNOR, J. A., AND LLINÁS, R. R. Spatially resolved calcium dynamics of mammalian Purkinje cells in cerebellar slice. *Science Wash. DC* 242: 773–777, 1988.

THOMPSON, A. M. Inhibitory postsynaptic potentials evoked in thalamic neurones by stimulation of the reticularis nucleus evoke slow spikes in isolated rat brain slice. I. *Neuroscience* 25: 491–502, 1988.

TSIEN, R. W., FOX, A. P., HESS, P., MCCLESKEY, E. W., NILIUS, B., NOWYCKY, M. C., AND ROSENBERG, R. L. Multiple type of calcium channel in excitable cells. In: *Society of General Physiologists Series. Proteins of Excitable Membranes,* edited by B. Hille and D. M. Fambrough. New York: Wiley, 1987, vol. 41, p. 167–188.

VERGNES, M., MARESCAUX, C., AND DEPAULIS, A. Mapping of spontaneous spike and wave discharges in Wistar rats with genetic generalized non-convulsive epilepsy. *Brain Res.* 523: 87–91, 1990.

VERGNES, M., MARESCAUX, C., DEPAULIS, A., MICHELETTI, G., AND WARTER, J. M. Spontaneous spike and wave discharges in thalamus and cortex in a rat model of genetic petit mal-like seizures. *Exp. Neurol.* 96: 127–136, 1987.

WESTENBROEK, R. E., AHLIJANIAN, M. K., AND CATTERALL, W. A. Clustering of L-type Ca^{2+} channels at the base of major dendrites in hippocampal pyramidal neurons. *Nature Lond.* 347: 281–284, 1990.

WOLLNER, D. A. AND CATTERALL, W. A. Localization of sodium channels in axon hillocks and initial segments of retinal ganglion cells. *Proc. Natl. Acad. Sci. USA* 83: 8424–8428, 1986.